

LayoutDETR: Detection Transformer Is a Good Multimodal Layout Designer

Ning Yu Chia-Chih Chen Zeyuan Chen Rui Meng Gang Wu Paul Josel
 Juan Carlos Niebles Caiming Xiong Ran Xu
 Salesforce Research

{ning.yu, chiachih.chen, zeyuan.chen, ruimeng, gang.wu, pjosel,
 jniebles, cxiong, ran.xu}@salesforce.com

Abstract

Graphic layout designs play an essential role in visual communication. Yet handcrafting layout designs is skill-demanding, time-consuming, and non-scalable to batch production. Generative models emerge to make design automation scalable but it remains non-trivial to produce designs that comply with designers’ multimodal desires, i.e., constrained by background images and driven by foreground content. We propose LayoutDETR that inherits the high quality and realism from generative modeling, while reformulating content-aware requirements as a detection problem: we learn to detect in a background image the reasonable locations, scales, and spatial relations for multimodal foreground elements in a layout. Our solution sets a new state-of-the-art performance for layout generation on public benchmarks and on our newly-curated ad banner dataset. We integrate our solution into a graphical system that facilitates user studies, and show that users prefer our designs over baselines by significant margins. Our code, models, dataset, graphical system, and demos are available at [GitHub](#).

1. Introduction

Graphic layout designs are at the foundation of communication between media designers and their target audience [40, 53, 73]. Multimodal elements, i.e. foreground images/texts, are framed by layout bounding boxes and reasonably arranged on a background image. This relies on a thoughtful understanding of the semantics of each element and their harmony as a whole. Therefore, handcrafting such layout designs is skill-demanding, time-consuming, and requires experienced professionals. In practice, it has been impossible to batch-produce them in massive quantities [12].

Growing demands of automating graphic layout designs have motivated researchers to adapt deep generative models [13, 18, 36, 41, 66] to this task [8, 14, 19, 20, 34, 38, 48, 60, 88, 90], but few of them investigate generation conditioned

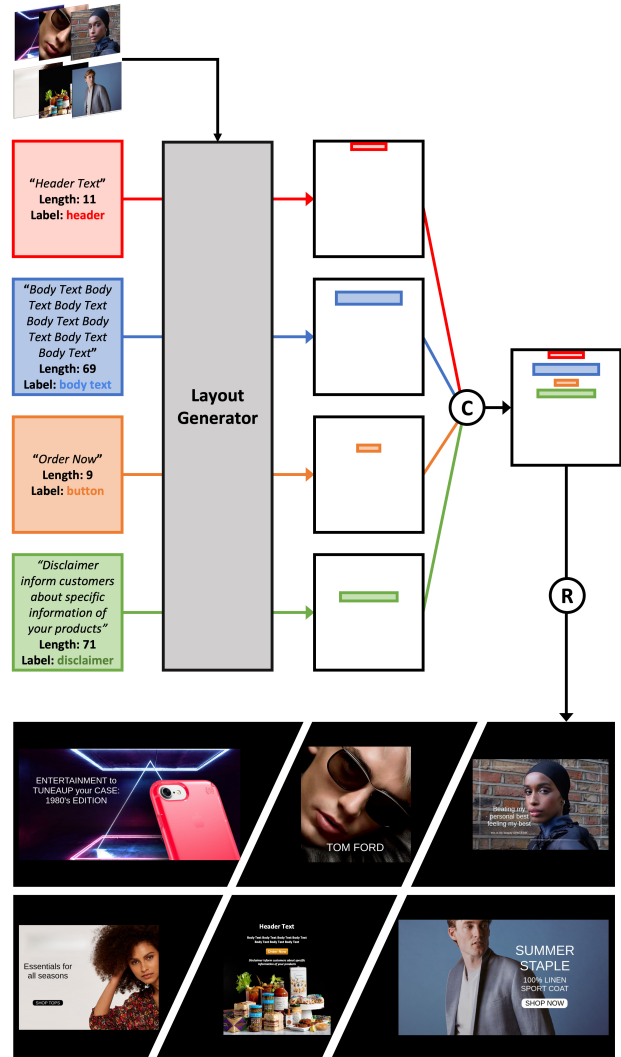


Figure 1. **Top:** LayoutDETR takes a background image and a set of multimodal foreground elements (images/texts) as input, and outputs an aesthetically appealing layout. **Bottom:** we show a few banner samples with rendered texts using our auto-designed layouts. “C” is the composition and “R” the rendering process. on multimodal inputs and their fusion for layout designs.

Conditioning on multimodal inputs is critical to enrich designers’ control and to command the aesthetics of layout designs. In this paper, we focus on them. We propose to equip designers with an AI-empowered system that allows multimodal input: arbitrary background images, foreground images, and foreground copywriting texts from varying categories. Fig. 1 depicts the functionality and resulting design samples of our solution. We learn a generative model of conditional layout distribution that is constrained by background images and driven by foreground elements. This requires our model to (1) learn the prior distribution from large-scale realistic layout samples, (2) understand the appearance and semantics of background images, (3) understand the appearance and semantics of foreground elements, and (4) fuse background and foreground information to generate the layout bounding box parameters of each foreground element.

To tackle (1), we inherit and explore the high realism from three types of generative learning paradigms: generative adversarial networks (GANs) [18, 33], variational autoencoders (VAEs) [36], and VAE-GAN [41]. To handle (2), we reformulate the background conditioned layout generation as a detection problem, considering both problems require visual understanding of an image and optimize for bounding box parameters. We integrate these two seemingly irrelevant techniques and train a DETR-flavored detector [9] as a layout generator. Specifically, we employ the visual transformer encoder and bounding box transformer decoder architectures of DETR and jointly optimize its supervision loss with generative adversarial loss. We hence name our solution *LayoutDETR*. To handle (3), we incorporate a CNN-based image encoder [11] and a BERT-based text encoder [16] for the multimodal foreground inputs, and feed the features as input tokens to DETR transformer decoder. (4) is naturally handled by DETR thanks to its transformer nature: foreground elements interact with each other through the self-attention layers in the decoder, while background features interact through the cross-attention layers between the image encoder and layout decoder.

We summarize our **contributions** as: **(1) Method.** We bridge two seemingly irrelevant research domains, layout generation and visual detection, into one framework that solves multimodal graphic layout design constrained by background images and driven by foreground image/text elements. No existing methods can handle all these modalities at once. **(2) Dataset.** We establish a large-scale ad banner dataset with rich semantic annotations including text bounding boxes, text categories, and text content. We benchmark this dataset for graphic layout generation over six recent methods, three of our solution variants, and conduct ablation study. **(3) State-of-the-art performance.** Our solution reaches a new state-of-the-art performance for graphic layout generation in a comprehensive set of six

evaluation metrics, which measure the realism, accuracy, and regularity of generated layouts. **(4) Graphical system and user study.** We integrate our solution into a graphical system that scales up layout generation and facilitates user studies. We present generated layout samples (Fig. 1 bottom) to users. Users prefer our designs over all baselines by significant margins.

2. Related Work

Deep generative models for layout design. Automating the layout design with high quality and realism gains increasing attention and achieves substantial progress, thanks to the revolutionary advancements of deep generative models, especially generative adversarial networks (GANs) [7, 18, 31–33, 44, 68, 83–85], variational autoencoders (VAEs) [36, 41, 65], autoregressive models (ARMs) [13, 67, 76], and diffusion denoising probabilistic models (DDPM) [25, 58, 66, 72]. Researchers adopt generative models to learn to generate bounding box parameters, in the form of center location, height, width, and optionally depth, for each foreground element in a layout in either graphics or natural scene domains. Orthogonal to learning paradigms, existing methods also investigate a variety of generator architectures including multi-layer perceptron (MLP) [39], convolutional neural networks (CNN) [69], recursive neural networks (RvNN) [70, 71], long short-term memory (LSTM) [21, 26], graph convolutional networks (GCN) [37], transformer [16, 77], etc. Some layout design methods [5, 8, 10, 14, 19, 20, 28–30, 34, 38, 43, 45, 48, 49, 55–57, 60, 79–81, 88, 90] focus on graphics domain only, while others [5, 20, 30, 38, 42, 75, 87] generalize to natural scenes or even 3D data. Some methods [20, 34, 38, 45, 48, 60] allow only bounding box category condition, while others [8, 14, 19, 43, 49, 88, 90] allow richer conditions in multimodalities in the form of background images, foreground images, or foreground texts, but not all. A comprehensive taxonomy of layout generation methods is in Table 1.

None of the existing multimodal layout generation methods [8, 19, 43, 49, 88, 90] is designed to handle all the background and foreground modalities at once. LayoutGAN+ [49] and NDN [43] are unaware of background and foreground image elements in their formulation. CGLGAN [90] and ICVT [8] are unaware of foreground text and image elements in their formulation. ContentGAN [88] does not take layout spatial information for training and does not even use complete background images as input during training. This does not benefit the layout representation, layout regularity, or final quality (e.g., text readability) after rendering foreground elements onto the background. Vinci [19] relies on a finite set of predefined layout candidates to choose background images from a pool of food and beverage domains. Their method is unable to design layouts conditioned on arbitrary backgrounds in open domains, nat-

Method	Domain(s)	Conditioning modality	Generative model	Architecture
LayoutGAN [48]	Graphics	Bbox category	GAN	MLP, CNN
LayoutGAN+ [49]	Graphics	Bbox category, attribute vector	GAN	MLP, CNN
LayoutGAN++ [34]	Graphics	Bbox category	GAN	Transformer
House-GAN [55]	Floor plans	Bubble diagram	GAN	CNN, MPN [86]
House-GAN++ [56]	Floor plans	Bubble diagram	GAN	CNN, MPN [86]
LayoutVAE [30]	Natural scenes	Bbox category	VAE	MLP, LSTM
READ [60]	Graphics	Bbox category	VAE	RvNN
Vinci [19]	Graphics	Bbox category, bg/fg images, text	VAE	LSTM
NDN [43]	Graphics	Bbox category, spatial relation	VAE	GCN
VTN [5]	Graphics, natural scenes	Bbox category	VAE	Transformer
CanvasVAE [81]	Graphics	Bbox category, attribute vector	VAE	Transformer
C2F-VAE [29]	Graphics	Bbox category	VAE	Transformer
DeepSVG [10]	Vector graphics	Vector paths, attribute vector, command	VAE	Transformer
ContentGAN [88]	Graphics	Bbox category, fg image, text	VAE + GAN	Transformer
TextLogoLayout [79]	Graphics	Glyph	VAE + GAN	RNN, CNN
LayoutMCL [57]	Graphics	Bbox category	ARM	RNN, CNN
CanvasEmb [80]	Graphics	Bbox category, attribute vector	ARM	Transformer
LayoutTransformer [20]	Graphics, natural scenes, 3D	Bbox category	ARM	Transformer
BLT [38]	Graphics, natural scenes, 3D	Bbox category	ARM	Transformer
UniLayout [28]	Graphics	Bbox category	ARM	Transformer
PLay [14]	Graphics	Bbox category, guideline	Diffusion	Transformer
DLT [45]	Graphics	Bbox category	Diffusion	Transformer
CGL-GAN [90]	Graphics	Bg image	GAN + DETR	Transformer
ICVT [8]	Graphics	Bg image	VAE + DETR	Transformer
LayoutDETR-GAN (ours)	Graphics	Bbox category, bg/fg images, text	GAN + DETR	Transformer
LayoutDETR-VAE (ours)	Graphics	Bbox category, bg/fg images, text	VAE + DETR	Transformer
LayoutDETR-VAE-GAN (ours)	Graphics	Bbox category, bg/fg images, text	VAE + GAN + DETR	Transformer

Table 1. A taxonomy of existing and our layout generation methods. We tag for each method its working data domain(s), data modality(ies) of input condition(s), backend generative model type, as well as implementation architecture. Our method and its variants are the only ones that enable full control of varying multimodal conditions, and only a few that integrate object detection techniques into layout generation.

ural or handcrafted, plain or cluttered, like ours. Considering multimodal layout design persists as a challenging problem, we focus our scope on graphic layouts: mobile application UIs and our newly-organized large-scale ad banners. **Object detection.** The goal of object detection is to predict a set of bounding boxes and their categories for each object of interest in a query image. Modern detectors address this in one of three ways: Two-stage detectors [17, 23, 63] predict boxes based on proposals; single-stage detectors predict boxes based on anchors [50] or a grid of possible object centers [61, 62]; direct detectors [9, 15, 52, 54] avoid those hand-crafted initial guesses and directly predict absolute parameters of boxes in the query images. Direct detectors [9, 15] inspire us to leverage their powerful image understanding capability, and combine it with modern layout generators, in order to address the problem of multimodal layout generation. Similar in spirit to CGL-GAN [90] or ICVT [8], we take advantage of the transformer encoder-decoder architecture and generalized intersection over union (gIoU) loss [64] in DETR [9] to learn layout distributions from background image contexts. Unlike prior art, our layout outputs are additionally conditioned on foreground image/text elements.

3. LayoutDETR

Problem statement. A graphic layout sample \mathcal{L} is represented by a set of N 2D bounding boxes $\{\mathbf{b}^i\}_{i=1}^N$. Each

\mathbf{b}^i is parameterized by a vector with four elements: its center location in a background image (y^i, x^i) , height h^i , and width w^i . In order to handle background images \mathbf{B} with arbitrary sizes (H, W) , we normalize box parameters by their image size correspondingly, i.e., $\mathcal{L} = \{(y^i/H, x^i/W, h^i/H, w^i/W)\}_{i=1}^N \doteq \{\hat{\mathbf{b}}^i\}_{i=1}^N$. The multimodal inputs are the background image \mathbf{B} and a set of N foreground elements, in the form of either text elements $\mathcal{T} = \{\mathbf{t}^i\}_{i=1}^M = \{(s^i, c^i, l^i)\}_{i=1}^M$ or image patches $\mathcal{P} = \{\mathbf{p}^i\}_{i=1}^K$, where $M \geq 0, K \geq 0, M + K = N$. s^i is a text string, c^i is the text class from the set $\{\text{header text}, \text{body text}, \text{disclaimer text}, \text{button text}\}$, and l^i is the length of the text string. Each foreground element corresponds to a bounding box in the layout, indicating its location and size. In case there are foreground elements that we are not interested in, e.g., button underlays or embellishments, we leave them as part of the background. Our goal is to learn a layout generator G that takes a latent noise vector \mathbf{z} and the multimodal conditions as input, and outputs a realistic and reasonable layout complying with the multimodal control: $G(\mathbf{z}, \mathbf{B}, \mathcal{T} \cup \mathcal{P}) \mapsto \mathcal{L}_{\text{fake}}$.

3.1. Generative Learning Frameworks

GAN variant. Following the GAN paradigm [7, 18, 31–33, 44, 68, 83–85], the generator G is simultaneously and adversarially trained against discriminator D training. We formulate a multimodal-conditional discriminator $D^c(\mathcal{L}, \mathbf{B}, \mathcal{T} \cup$

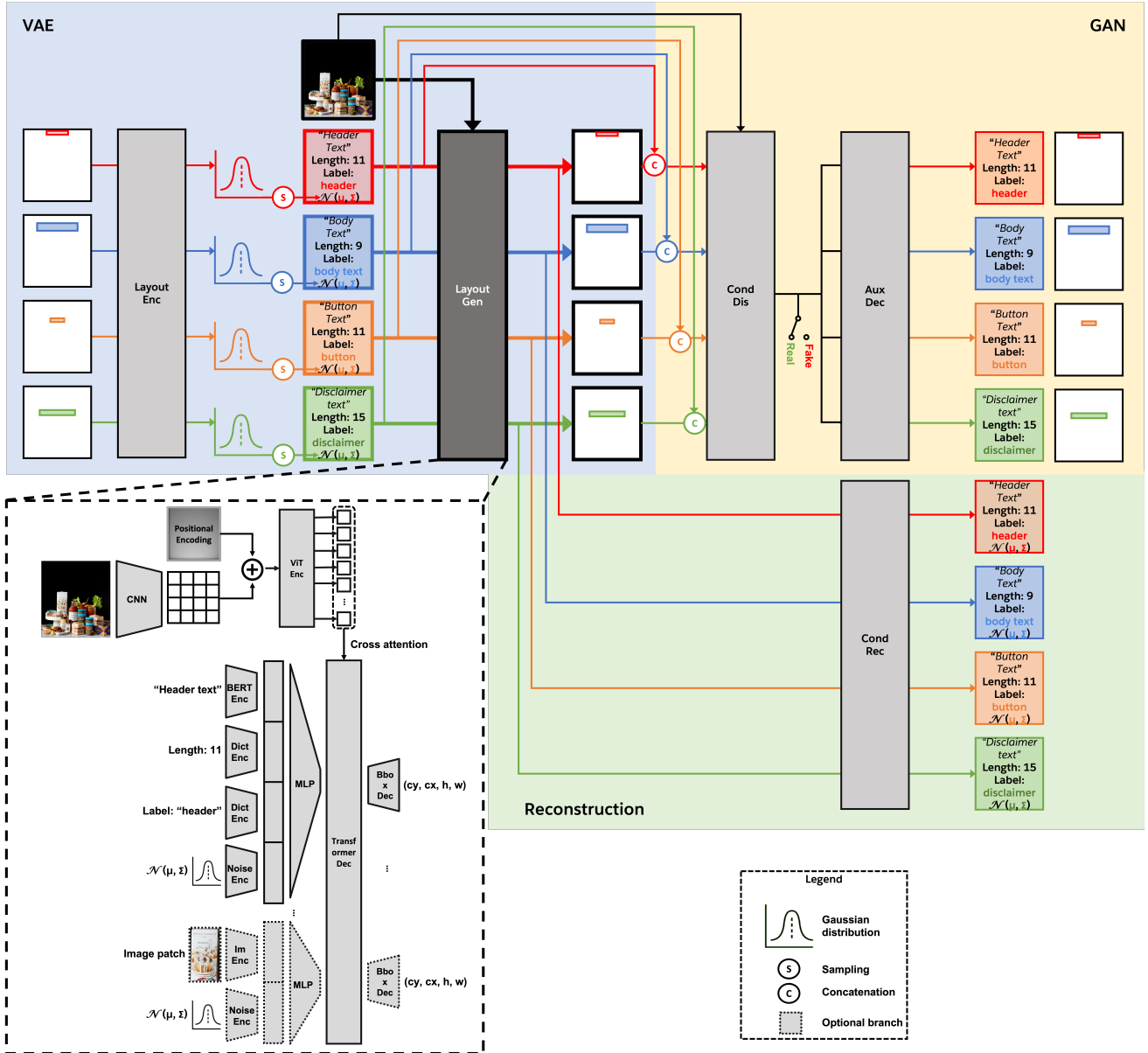


Figure 2. Our unified training framework covers three generator variants: GAN-, VAE-, and VAE-GAN-based. The layout generator network (darker color and bold) appears in all variants. Its DETR-based multimodal architecture is at the bottom left. During inference, only the generator is needed.

$\mathcal{P}) \mapsto \{0, 1\}$, as well as an unconditional discriminator $D^u(\mathcal{L}) \mapsto \{0, 1\}$. The use of conditional discriminator D^c is straightforward due to the nature of our multimodal conditions: it encourages foreground elements to be harmonic and reasonable to the background after being overlaid according to the generated layout. The unconditional discriminator D^u differs from D^c by ignoring background and foreground elements, and focusing only on the realism of layouts themselves. Therefore, the use of D^u additionally encourages the mutual relations among bounding boxes in a generated layout to be realistic and reasonable, regardless of multimodal conditions. The empirical effectiveness of

D^u is evidenced in Table 2 Row 3.

It has been observed that the discriminators are insensitive to irregular bounding box positions [34]. For example, the discriminators tend to overlook the unusual layout where a *header texts* is placed at the bottom. As a result, we follow the self-learning technique in [51] and add position-aware regularization to our discriminators. Similar to [34], we add an auxiliary decoder to each discriminator to reconstruct its input. The decoders F^c/F^u take the output features f^c/f^u of their discriminators D^c/D^u , add them with learnable positional embeddings $\mathcal{E}^c = \{e_i^c\}_{i=1}^N / \mathcal{E}^u = \{e_i^u\}_{i=1}^N$, and reconstruct the bounding box parameters and multi-

modal conditions that are the input of the discriminators: $F^c(\mathbf{f}^c, \mathcal{E}^c) \mapsto \mathcal{L}_{\text{dec}}^c, \mathbf{B}_{\text{dec}}, \mathcal{T}_{\text{dec}} \cup \mathcal{P}_{\text{dec}}$; $F^u(\mathbf{f}^u, \mathcal{E}^u) \mapsto \mathcal{L}_{\text{dec}}^u$. F^c/F^u targets to self-reconstruct all the input information of D^c/D^u through the bottleneck discriminator features. It encourages the input information to be fully encoded into the discriminator features such that the discriminator classification is fully justified by the input. The empirical effectiveness of F^c/F^u has been validated in [34] Table 2 last column.

The decoders are jointly trained with the discriminators to minimize the reconstruction loss. See Fig. 2 Yellow for the diagram. Thus, our adversarial learning objective is:

$$\min_G \max_{D^c, F^c, \mathcal{E}^c, D^u, F^u, \mathcal{E}^u} L_{\text{GAN}} = L_{\text{GAN, fake}} + L_{\text{GAN, real}} \quad (1)$$

$$L_{\text{GAN, fake}} \doteq \mathbb{E}_{\mathbf{z} \sim \mathcal{N}(\mathbf{0}, \mathbf{I}), \{\mathbf{B}, \mathcal{T} \cup \mathcal{P}\} \sim P_{\text{data}}} \left[\log(1 - D^c(\mathcal{L}_{\text{fake}}, \mathbf{B}, \mathcal{T} \cup \mathcal{P})) + \log(1 - D^u(\mathcal{L}_{\text{fake}})) \right] \quad (2)$$

$$L_{\text{GAN, real}} \doteq \mathbb{E}_{\{\mathcal{L}_{\text{real}}, \mathbf{B}, \mathcal{T} \cup \mathcal{P}\} \sim P_{\text{data}}} \left[\log(D^c(\mathcal{L}_{\text{real}}, \mathbf{B}, \mathcal{T} \cup \mathcal{P})) + \log(D^u(\mathcal{L}_{\text{real}})) - L_{\text{dec}}(F^c(\mathbf{f}^c, \mathcal{E}^c), (\mathcal{L}_{\text{real}}, \mathbf{B}, \mathcal{T} \cup \mathcal{P})) - \lambda_{\text{layout}} L_{\text{layout}}(F^u(\mathbf{f}^u, \mathcal{E}^u), \mathcal{L}_{\text{real}}) \right] \quad (3)$$

$$L_{\text{dec}}((\mathcal{L}_1, \mathbf{B}_1, \mathcal{T}_1 \cup \mathcal{P}_1), (\mathcal{L}_2, \mathbf{B}_2, \mathcal{T}_2 \cup \mathcal{P}_2)) = \lambda_{\text{layout}} L_{\text{layout}}(\mathcal{L}_1, \mathcal{L}_2) + \lambda_{\text{im}} (\|\mathbf{B}_1 - \mathbf{B}_2\|_2 + L_{\text{im}}(\mathcal{P}_1, \mathcal{P}_2)) + L_{\text{text}}(\mathcal{T}_1, \mathcal{T}_2) \quad (4)$$

$$L_{\text{layout}}(\mathcal{L}_1, \mathcal{L}_2) = \frac{1}{N} \sum_{i=1}^N \|\hat{\mathbf{b}}_1^i - \hat{\mathbf{b}}_2^i\|_2 \quad (5)$$

$$L_{\text{im}}(\mathcal{P}_1, \mathcal{P}_2) = \frac{1}{N} \sum_{i=1}^N \|\mathbf{p}_1^i - \mathbf{p}_2^i\|_2 \quad (6)$$

$$L_{\text{text}}(\mathcal{T}_1, \mathcal{T}_2) = \frac{1}{N} \sum_{i=1}^N (\lambda_{\text{str}} L_{\text{str}}(\mathbf{s}_1, \mathbf{s}_2) + \lambda_{\text{cls}} L_{\text{cls}}(c_1, c_2) + \lambda_{\text{len}} L_{\text{len}}(l_1, l_2)) \quad (7)$$

where $L_{\text{str}}, L_{\text{cls}}, L_{\text{len}}$ are the reconstruction losses for foreground text strings, text classes, and text lengths respectively. L_{str} is the auto-regressive loss according to BERT

language modeling [16, 47]. L_{cls} is the standard classification cross-entropy loss. So is L_{len} , considering we quantize and classify a string length integer into one of 256 levels [0, 255]. $\lambda_{\text{layout}} = 500.0$, $\lambda_{\text{im}} = 0.5$, $\lambda_{\text{str}} = 0.1$, $\lambda_{\text{cls}} = 50.0$, and $\lambda_{\text{len}} = 2.0$ are set to calibrate the scale of each loss term.

VAE variant. VAEs are an alternative paradigm to GANs for generative models. Following the VAE paradigm [36, 65], the generator G is jointly trained with an encoder E that maps from the layout space to the latent noise distribution space. The output of E are the mean μ and covariance matrix Σ of a multivariate Gaussian distribution, $E(\mathcal{L}) \mapsto \mu, \Sigma$, the samples of which are input to G : $\text{sample}(\mu, \Sigma) = \mathbf{z}_0^T \Sigma^{\frac{1}{2}} \mathbf{z}_0 + \mu$, $\mathbf{z}_0 \sim \mathcal{N}(\mathbf{0}, \mathbf{I})$. It represents the differentiable reparameterization trick in the standard VAE pipeline [36, 65]. See Fig. 2 Blue.

The conditional VAE minimizes the reconstruction loss:

$$\min_{E, G} L_{\text{VAE}} \doteq \mathbb{E}_{\{\mathcal{L}_{\text{real}}, \mathbf{B}, \mathcal{T} \cup \mathcal{P}\} \sim P_{\text{data}}} \left[\lambda_{\text{layout}} L_{\text{layout}}(\mathcal{L}_{\text{fake}}, \mathcal{L}_{\text{real}}) + \lambda_{\text{KL}} \text{KL}(E(\mathcal{L}_{\text{real}}) \parallel \mathcal{N}(\mathbf{0}, \mathbf{I})) \right] \quad (8)$$

$\text{KL}(\cdot \parallel \cdot)$ is the Kullback-Leibler (KL) Divergence used in standard VAE [36, 65] to regularize the encoded latent noise distribution. The hyper-parameters $\lambda_{\text{layout}} = 500.0$ and $\lambda_{\text{KL}} = 1.0$.

VAE-GAN variant. VAEs and GANs are compatible and complementary to each other in terms of data distribution learning and feature representation learning [41]. Inspired by [88], we combine the strengths of VAEs and GANs and apply them for layout generation. See Fig. 2 Blue plus Yellow in the diagram. As suggested by [41, 88], we jointly optimize Eq. 1 and 8:

$$\min_{E, G} \max_{D^c, F^c, \mathcal{E}^c, D^u, F^u, \mathcal{E}^u} L_{\text{GAN}} + L_{\text{VAE}} \quad (9)$$

3.2. Additional Objectives

Other losses and regularization terms also play important roles in the generated layout quality. First, we add bounding box supervision as in DETR [9]. We use the generalized intersection over union loss $\text{gIoU}(\cdot, \cdot)$ [64] between generated layout and its ground truth $L_{\text{gIoU}}(\mathcal{L}_{\text{fake}}, \mathcal{L}_{\text{real}})$, where:

$$L_{\text{gIoU}}(\mathcal{L}_1, \mathcal{L}_2) \doteq \lambda_{\text{gIoU}} \frac{1}{N} \sum_{i=1}^N \text{gIoU}(\hat{\mathbf{b}}_1^i, \hat{\mathbf{b}}_2^i) \quad (10)$$

where the hyper-parameter $\lambda_{\text{gIoU}} = 4.0$.

Second, we introduce an auxiliary reconstructor R for the generator to enhance the controllability of input conditions. R takes the last features of G , $\mathcal{F} = \{\mathbf{f}_i^g\}_{i=1}^N$, as input tokens before outputting box parameters, and learns to reconstruct \mathcal{P} and \mathcal{T} : $R(\mathcal{F}) \mapsto \mathcal{P}_{\text{rec}}, \mathcal{T}_{\text{rec}}$.

Jointly with G training, we learn to minimize:

$$L_{\text{rec}} \doteq \lambda_{\text{im}} L_{\text{im}}(\mathcal{P}_{\text{rec}}, \mathcal{P}_{\text{real}}) + L_{\text{text}}(\mathcal{T}_{\text{rec}}, \mathcal{T}_{\text{real}}) \quad (11)$$

with L_{im} from Eq. 6 and L_{text} from 7. See Fig. 2 Green. The use of R following G stems from the same motivation as the use of auxiliary decoders F^c/F^u . Its empirical effectiveness is evidenced in Table 2 Row 2.

Third, reasonable layout designs typically avoid overlapping between foreground elements. We leverage the overlap loss $L_{\text{overlap}} \doteq \lambda_{\text{overlap}} L_{\text{overlap}}(\mathcal{L}_{\text{fake}})$ from [49] that discourages overlapping between any pair of bounding boxes in a generated layout. The hyper-parameter $\lambda_{\text{overlap}} = 7.0$.

Fourth, aesthetically appealing layouts usually maintain one of the six alignments between a pair of adjacent bounding boxes: left, horizontal-center, right, top, vertical-center, and bottom aligned. We leverage the misalignment loss $L_{\text{misalign}} \doteq \lambda_{\text{misalign}} L_{\text{misalign}}(\mathcal{L}_{\text{fake}})$ follow [49] that discourages misalignment. We set $\lambda_{\text{misalign}} = 17.0$.

Finally, our training objective is formulated as follows:

$$\min_{E, G, R} \max_{D^c, F^c, \mathcal{E}^c, D^u, F^u, \mathcal{E}^u} L_{\text{GAN}} + L_{\text{VAE}} + L_{\text{gIoU}} + L_{\text{rec}} + L_{\text{overlap}} + L_{\text{misalign}} \quad (12)$$

3.3. DETR-based Multimodal Architectures

Architecture design is where we integrate object detection with layout generation. Detection transformer (DETR) [9] is employed and modified for LayoutDETR generator G and conditional discriminator D^c .

As depicted in Fig. 2 bottom left, G and D^c contain a background encoder and a layout transformer decoder. The encoder is the same as in DETR [9]. The decoder is inherited from the DETR decoder with self-attention and encoder-decoder-cross-attention mechanisms [77]. Different from DETR, we replace their freely-learnable object queries with our foreground embeddings as the input tokens to the decoder. The decoder then transforms the embeddings to layout bounding box parameters. Foreground embedding is a concatenation of noise embedding and text/image embedding. Text embedding is a concatenation of text string embedding (BERT-pretrained and fixed), text class embedding (via learning dictionary), and text length embedding (via learning dictionary).

The motivation of using DETR architecture [9] for background image encoding and understanding stems from its state-of-the-art performance for object detection using the state-of-the-art visual transformer (ViT) encoder architecture [22, 78]. In our scenarios, “detection” is equivalent to “generation” as both processes output bounding box parameters. Although “detection” lacks the “layout” concept, it is complemented by the layout discriminator and encoder networks. “Object” stands for the non-clutter subregions in a background that are suitable for overlaying foreground elements. ViT tokenizes visual features that facilitate cross attention with other foreground element features, e.g., tokenized text features, so that multimodal conditions can synergize jointly.

See more details and implementations of the other networks in the supplementary material. In particular, other networks are transformer-based as well. Only the input and output formats differ depending on the network functionality. We do not choose a wire-frame discriminator since its empirical performance is worse, as also observed in [34].

4. New Ad Banner Dataset

Not all existing datasets are suitable for multimodal layout design because they do not always provide multimodality information, e.g. natural scene datasets or Crello graphic document dataset [81]. Other datasets, such as PubLayNet document dataset [89] and PartNet 3D shape dataset [82] render layouts only on plain background. Magazine dataset [88] does not provide complete background images since they have masked out foreground layouts from the background. On the other hand, ad banner datasets are composed of multimodal elements and lead to several previous layout design techniques [8, 19, 38, 43, 79, 90]. Unfortunately, none of their datasets is publicly available, except for CGL dataset [90] and TextLogoLayout dataset [79] which yet do not contain English modality. We therefore collect a new large-scale ad banner dataset of 7,196 samples containing English characters, which are ready to release.

Each of our samples consists of a well-designed banner image, its layout ground truth, foreground text strings, text classes, and background image. The banner images are filtered from Pitt Image Ads Dataset [27] and crawled from Google Image Search Engine. Their layouts and text classes are manually annotated by Amazon Mechanical Turk (AMT). The text classes are $\{\text{header text}, \text{body text}, \text{disclaimer text}, \text{button text}\}$, with logos categorized as *header text*. The text strings are extracted by OCR [1] and removed by image inpainting [74] to obtain the text-free background image. Examples and more details about data collection are in the supplementary material.

5. Experiments

Datasets. Ablation study and user study are conducted on our newly-curated ad banner dataset with 7,196 samples. Comparisons to baselines are additionally performed on the CGL dataset with 59,978 valid Chinese ad banner samples [90], and on the CLAY dataset with 32,063 valid mobile application UI samples [46]. We apply the same OCR and image inpainting processes to CGL and CLAY datasets, in order to extract texts as part of input conditions, and separate between foreground and background. 90% of the samples are used for training and 10% for testing.

Baselines. We select six recent methods covering a variety of generative paradigms and architectures: LayoutGAN++ [34] (GAN paradigm, transformer architecture), READ [60] (VAE paradigm, RvNN architecture), Vinci [19] (VAE paradigm, LSTM architecture), LayoutTransformer [20] (ARM paradigm, transformer ar-

Method	Realism		Accuracy		Regularity	
	Layout FID ↓	Image FID ↓	IoU ↑	DocSim ↑	Overlap ↓	Misalign ($\times 10^{-2}$) ↓
Conditional LayoutGAN++	4.25	28.40	0.163	0.130	0.104	0.759
+ Gen. rec. (Eq. 11)	3.27	29.56	0.186	<u>0.148</u>	0.125	0.853
+ Uncond. dis. D^u	3.70	29.21	0.177	0.140	<u>0.103</u>	<u>0.681</u>
+ gIoU loss (Eq. 10)	<u>3.23</u>	<u>28.20</u>	0.182	0.138	0.106	0.721
+ Overlap & Misalign loss = LayoutDETR-GAN (ours)	3.19	27.35	0.208	0.151	0.101	0.646
- Text length embeddings	3.24	28.65	<u>0.191</u>	0.144	0.117	0.807
- Text class embeddings	25.17	29.25	0.166	0.132	0.110	0.000

Table 2. Ablation study w.r.t. loss config (top) or conditional embedding config (bottom) on **our ad banner dataset**. Each row is progressively ablated from its row above. \uparrow/\downarrow indicates a higher/lower value is better. **Bold/underline** font indicates the top/second best value in the column.

chitecture), CGL-GAN [90] (GAN + DETR paradigm, transformer architecture), and ICVT [8] (VAE + DETR paradigm, transformer architecture). We noted that LayoutTransformer [20] is empirically superior to the more recent work BLT [38], the same observation as Row 1 v.s. Row 8 in Table 2 of [28]. We therefore did not experiment with BLT.

Evaluation metrics. (1) For the **realism** of generated layouts, we calculate the Fréchet distances [24] between fake and real feature distributions. We consider two feature spaces: the layout features pretrained by [34], and VGG image features pretrained on ImageNet [24]. We obtain the output banner images by overlaying foreground image patches and rendering foreground texts on top of background images according to the generated layout. The rendering process and examples are in Fig. 4. (2) For the sample-wise **accuracy** of generated layouts w.r.t. their ground truth, we calculate the layout-to-layout IoU [34] and DocSim [60]. Box-level matching is trivial as the correspondences between generated and ground truth boxes are given by the conditioning input. (3) For the **regularity** of generated layouts, our metrics are the overlap loss [49] and misalignment loss [49] in Section 3.2.

5.1. Ablation Study

Loss configurations. We start from the LayoutGAN++ [34] baseline implementation and additionally enable it to take multimodal foreground and background as input conditions. We then progressively add on extra loss terms and report the quantitative measurements in Table 2 top section. We observe:

- (1) Comparing Row 1 and 2, all the metrics are improved, thanks to the enhanced controllability through the reconstruction of conditional inputs.
- (2) Comparing Row 2 and 3, unconditional discriminator benefits the layout regularity due to its approximation power between generated layout parameters and real regular ones.
- (3) Comparing Row 3 and 4, the supervised gIoU loss boosts the realism and accuracy by a significant margin, yet seemingly contradicts the regularity.
- (4) Fortunately, in Row 5, adding overlap loss and mis-

Method	Realism		Accuracy		Regularity	
	Layout FID ↓	Image FID ↓	IoU ↑	DocSim ↑	Overlap ↓	Misalign ($\times 10^{-2}$) ↓
Our ad banner dataset						
LayoutGAN++ [34]	4.25	28.40	0.163	0.130	0.104	0.759
READ [60]	4.45	32.10	0.177	0.141	0.093	2.867
Vinci [19]	38.97	58.12	0.104	0.143	0.243	0.271
LayoutTransformer [20]	5.47	39.70	0.080	0.115	0.127	3.632
CGL-GAN [90]	4.69	30.50	0.154	0.127	0.116	1.191
ICVT [8]	12.54	30.11	0.163	0.137	0.423	0.682
LayoutDETR-GAN (ours)	3.19	27.35	0.208	<u>0.151</u>	<u>0.101</u>	<u>0.646</u>
LayoutDETR-VAE (ours)	3.25	27.47	0.216	0.152	0.119	1.737
LayoutDETR-VAE-GAN (ours)	<u>3.23</u>	27.88	<u>0.210</u>	<u>0.151</u>	0.117	1.439
CGL Chinese ad banner dataset						
LayoutGAN++ [34]	11.43	11.92	0.061	0.083	0.593	0.729
READ [60]	10.51	6.58	0.269	0.127	0.145	0.704
Vinci [19]	12.06	5.38	<u>0.266</u>	<u>0.125</u>	0.093	0.433
LayoutTransformer [20]	5.11	4.65	0.186	0.114	0.340	0.276
CGL-GAN [90]	5.63	7.26	0.107	0.093	0.297	0.538
ICVT [8]	10.76	4.22	0.169	0.109	0.327	<u>0.340</u>
LayoutDETR-GAN (ours)	2.40	<u>4.11</u>	0.157	0.106	0.187	0.464
LayoutDETR-VAE (ours)	8.57	4.21	0.208	0.120	0.288	0.374
LayoutDETR-VAE-GAN (ours)	<u>2.65</u>	2.66	0.180	0.110	<u>0.134</u>	0.401
CLAY mobile application UI dataset						
LayoutGAN++ [34]	14.12	7.49	0.049	0.078	0.817	1.057
READ [60]	3.68	5.38	<u>0.312</u>	<u>0.121</u>	<u>0.099</u>	2.045
Vinci [19]	22.98	13.04	0.178	0.104	0.253	2.526
LayoutTransformer [20]	<u>2.64</u>	5.27	0.216	0.106	0.357	0.833
CGL-GAN [90]	47.74	8.96	0.034	0.066	1.153	1.099
ICVT [8]	4.56	<u>5.26</u>	0.208	0.105	0.396	1.066
LayoutDETR-GAN (ours)	1.84	5.22	0.261	0.113	0.083	<u>0.773</u>
LayoutDETR-VAE (ours)	4.99	5.49	0.327	0.123	0.205	5.119
LayoutDETR-VAE-GAN (ours)	3.98	5.87	0.158	0.108	0.148	0.691

Table 3. Quantitative comparisons to baselines. \uparrow/\downarrow indicates a higher/lower value is better. **Bold/underline** font indicates the top/second best value in the column.

alignment loss optimizes all the metrics. We name this "LayoutDETR-GAN (ours)" and stick to it for the following experiments.

Conditional embedding configurations. We do not consider foreground images in this ablation study as the embeddings are simply image features. Whereas for foreground texts, we examine the importance of text length embeddings and text class embeddings by progressively removing them from the training. From Table 2 bottom section we observe: (1) Comparing Row 5 and 6, text length embeddings are beneficial all around. We reason that text length is a strong indicator of a proper text box size. This validates the strong positive correlation between text lengths and box sizes. (2) Comparing Row 6 and 7, text label embeddings serve as an essential role in the generation. LayoutFID deteriorates significantly without text label embeddings (Row 7) as boxes of similar texts tend to collapse to the same regions (referring to the 0.0 misalignment). This implies that text content itself is not as discriminative as text labels to differentiate box parameters. This also explains why a variety of layout datasets and models have to involve box labels.

5.2. Comparisons to baselines

Quantitative comparisons are in Table 3. We test three of our alternative model variants: GAN-, VAE-, and VAE-GAN-based. For intuitive understanding of the tables, we visualize each row into a radar plot in Fig. 3. Each corner of the radar plot corresponds to a metric. We observe:

- (1) On our ad banner dataset, at least one of our variants outperforms all the baselines in terms of realism and ac-

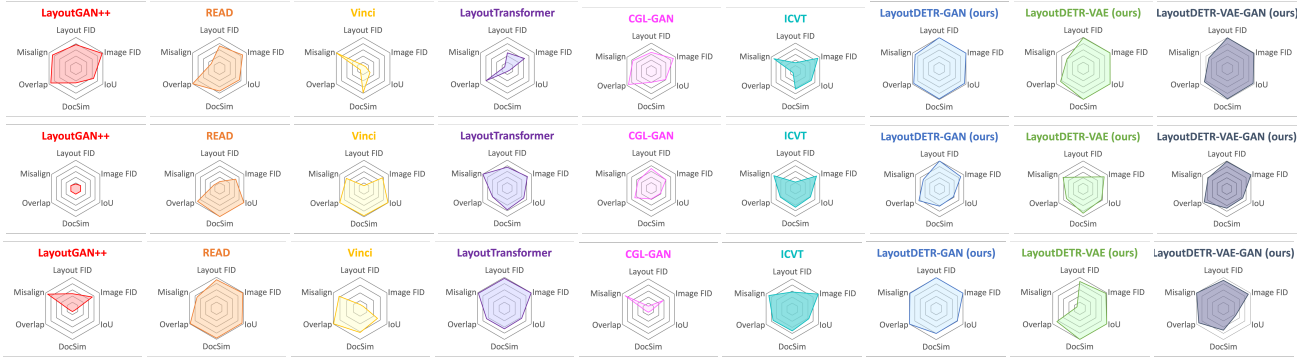


Figure 3. Radar plots for Table 3 on **our ad banner dataset (top)**, **CGL Chinese ad banner dataset (middle)**, and **CLAY mobile application UI dataset (bottom)**. Each plot corresponds to a row (method) in the table. Each corner in a plot corresponds to a column (metric) in the table. Values are normalized to the unit range, the higher the better.

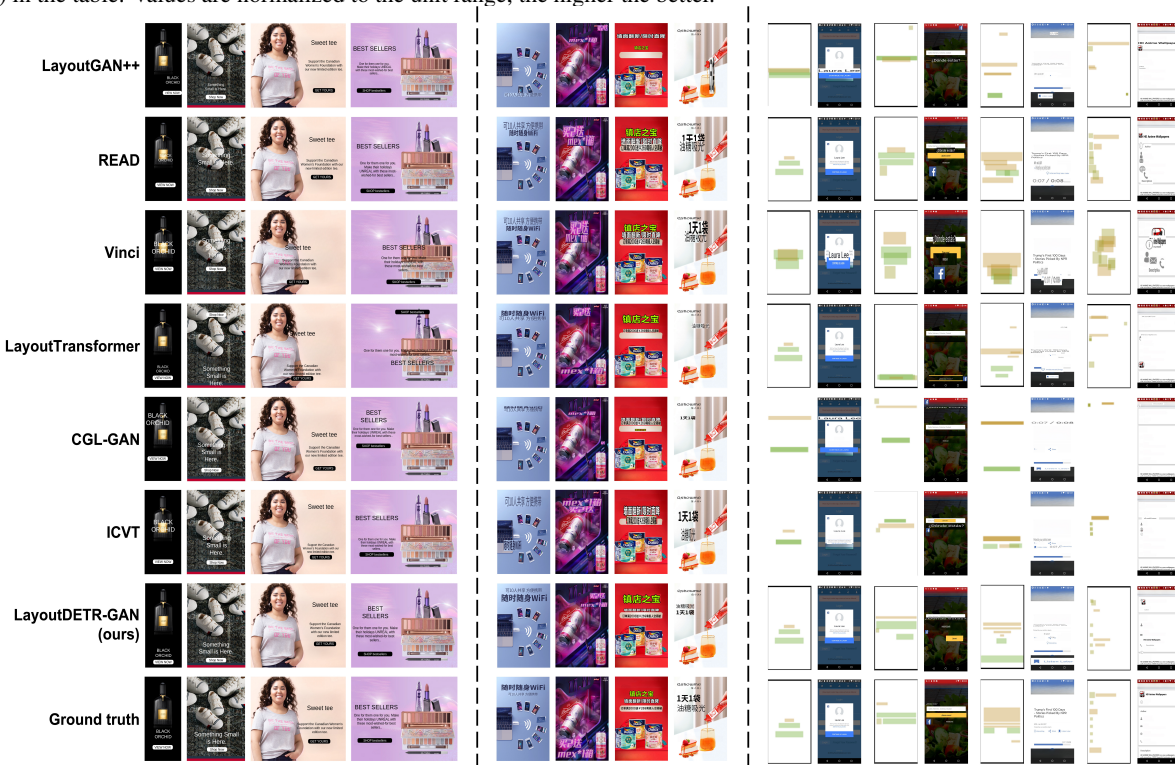


Figure 4. **Left:** comparisons on the testing set of **our ad banner dataset**. We apply the same rendering process to all methods: (1) Text font sizes and line breakers are adaptively determined to tightly fit into their inferred boxes. (2) Text font colors and button pad colors are adaptively determined to be either black or white whichever contrasts more with the background. (3) Button text colors are then determined to contrast with the button pads. (4) Text font is set to *Arial*. (5) Boxes are enforced to horizontally center-align with each other. **Middle:** comparisons on **CGL Chinese ad banner dataset**. Image patches that contain foreground text elements are resized and overlaid on the background following the generated layouts. **Right:** comparisons on **CLAY mobile application UI dataset**.

curacy. Our LayoutDETR-GAN achieves the second best in terms of regularity. The margin to the best baseline is minor. This evidences the efficacy of our understanding of multi-modality and sophisticated loss configurations.

(2) On CGL Chinese ad banner dataset, our variants lead in the most important realism metrics by significant margins. LayoutTransformer achieves a similarly balanced performance. READ and Vinci lead in the accuracy metrics yet significantly underperform in at least one other metric.

(3) On CLAY dataset, at least one of our variants outperforms all the baselines in all metrics. Our efficacy generalizes in at least these two multimodal foreground domains: texts and images.

(4) By overviewing the radar plots on all three datasets, our LayoutDETR-GAN variant (the third to the right) achieves near-top overall measures with the most balanced performance and without shortcomings. We therefore apply this variant for the following system design and user study. All

baselines miss at least one measurement by a significant margin on at least one dataset. This is due to their generators by nature not being designed for multimodal conditions.

Qualitative comparisons are in Fig. 4. We observe:

(1) For our and CGL ad banner datasets, our designs understand the background the most effectively. For example, they never overlay foreground elements on top of clutter background subregions. If the background looks symmetric, our layouts are placed in the middle of the banners.

(2) For these two datasets, our designs also approximate the real layout distribution the most closely, in terms of the relative font sizes (box sizes) and spatial relations (box orders and distances). Even for samples not close to their ground truth, our design variants still look the most reasonable and most harmonic together with backgrounds.

(3) CLAY dataset is more challenging in terms of multimodal conditioning, as it has more tiny foreground elements. Still, our layouts appear the best aligned and least overlapping, with reasonable designs to harmonize with backgrounds, although different from the ground truth.

The supplement material shows more uncurated results, including the impact of varying texts on layouts and our limitation in challenging scenarios.

5.3. Graphical System Design and User Study

We integrate our generator into a graphical system for user-friendly utilization in practice. See the details of UI design in the supplementary material.

With the graphical system, we can test a massive number of cases and collect generation results in the wild. This facilitates us to analyze users’ subjective preferences for our designs. In specific, we tested on 308 ad banner samples by rendering our designs and baseline designs via the graphical system. We configured a binary comparison task between our result and each of the baseline results for each sample. We intentionally avoided comparisons among more than two methods. This is because (1) we are not interested in the comparisons among baselines, and (2) extra unnecessary complexity would distract users’ attention. In total, we launched $308 \times 6 = 1,848$ jobs on AMT, and randomly assigned three workers for each job. We simply asked each worker which of the two designs they prefer. We intentionally did not pre-define any criterion for the preference so as to fully respect their subjective judgments. All workers have an approval rate history above 90% on AMT. We did not set any restrictions for workers’ gender, race, sexuality, demographics, locations, remuneration rates, etc. Our user study has been reviewed and approved by our ethical board.

Table 4 lists the ratio of users that prefer our designs over each baseline. To quantify the statistical significance of our user study, we calculate the p-value of a null hypothesis that the results of binary comparisons are equivalent to tossing a fair coin. We calculate it via the cumulative distribution function of the binomial distribution, the smaller the

Method	Ratio of preferences to LayoutDETR-GAN (ours)	p-value for statistical significance
LayoutGAN++ [34]	55.7%	2e-4
READ [60]	54.2%	5e-3
Vinci [19]	62.6%	3e-15
LayoutTransformer [20]	63.5%	2e-17
CGL-GAN [90]	54.7%	3e-3
ICVT [8]	55.4%	6e-4

Table 4. Two-way user preferences on **our ad banner dataset** between our method and baselines.

more statistically significant. In Table 4 all ratios are above 50%: a majority of users prefer our designs over any baseline. These preferences are statistically significant, as all p-values $\ll 0.05$. This validates that our layout designs are more appealing to users. We attribute this to our effective approximation of real layout distributions and understanding of multimodal conditions.

6. Conclusion

We present LayoutDETR for customizable layout design. It inherits the high quality and realism of generative models, and benefits from object detectors to understand multimodal conditions. Experiments show that we achieve a new state-of-the-art performance for layout generation on a new ad banner dataset and beyond. We implement our solution as a graphical system that facilitates user studies. Users prefer our designs over several recent works.

Acknowledgement

We thank Abigail Kuttruff, Brian Brechbuhl, Elham Etemad, and Amrutha Krishnan from Salesforce for constructive advice.

References

- [1] <https://github.com/PaddlePaddle/PaddleOCR>. 6, 14
- [2] <https://www.mturk.com/>. 13
- [3] <https://www.freepik.com/>. 17
- [4] <https://www.pmi.com/>. 18, 19
- [5] Diego Martin Arroyo, Janis Postels, and Federico Tombari. Variational transformer networks for layout generation. *CVPR*, 2021. 2, 3
- [6] Irwan Bello, Barret Zoph, Ashish Vaswani, Jonathon Shlens, and Quoc V Le. Attention augmented convolutional networks. *ICCV*, 2019. 13
- [7] Andrew Brock, Jeff Donahue, and Karen Simonyan. Large scale gan training for high fidelity natural image synthesis. *ICLR*, 2019. 2, 3
- [8] Yunning Cao, Ye Ma, Min Zhou, Chuanbin Liu, Hongtao Xie, Tiezheng Ge, and Yuning Jiang. Geometry aligned variational transformer for image-conditioned layout generation. *Multimedia*, 2022. 1, 2, 3, 6, 7, 9
- [9] Nicolas Carion, Francisco Massa, Gabriel Synnaeve, Nicolas Usunier, Alexander Kirillov, and Sergey Zagoruyko. End-to-end object detection with transformers. *ECCV*, 2020. 2, 3, 5, 6, 13

- [10] Alexandre Carlier, Martin Danelljan, Alexandre Alahi, and Radu Timofte. Deepsvg: A hierarchical generative network for vector graphics animation. *NeurIPS*, 2020. 2, 3
- [11] Mathilde Caron, Ishan Misra, Julien Mairal, Priya Goyal, Piotr Bojanowski, and Armand Joulin. Unsupervised learning of visual features by contrasting cluster assignments. 2020. 2
- [12] Gang Chen, Peihong Xie, Jing Dong, and Tianfu Wang. Understanding programmatic creative: The role of ai. *Journal of Advertising*, 2019. 1
- [13] Xi Chen, Nikhil Mishra, Mostafa Rohaninejad, and Pieter Abbeel. Pixelsnail: An improved autoregressive generative model. *ICML*, 2018. 1, 2
- [14] Chin-Yi Cheng, Forrest Huang, Gang Li, and Yang Li. Play: Parametrically conditioned layout generation using latent diffusion. *arXiv*, 2023. 1, 2, 3
- [15] Zhigang Dai, Bolun Cai, Yugeng Lin, and Junying Chen. Up-detr: Unsupervised pre-training for object detection with transformers. *CVPR*, 2021. 3, 13
- [16] Jacob Devlin, Ming-Wei Chang, Kenton Lee, and Kristina Toutanova. Bert: Pre-training of deep bidirectional transformers for language understanding. *NAACL*, 2019. 2, 5, 13
- [17] Ross Girshick. Fast r-cnn. *ICCV*, 2015. 3
- [18] Ian Goodfellow, Jean Pouget-Abadie, Mehdi Mirza, Bing Xu, David Warde-Farley, Sherjil Ozair, Aaron Courville, and Yoshua Bengio. Generative adversarial networks. *NeurIPS*, 2014. 1, 2, 3
- [19] Shunan Guo, Zhuochen Jin, Fuling Sun, Jingwen Li, Zhaorui Li, Yang Shi, and Nan Cao. Vinci: an intelligent graphic design system for generating advertising posters. *CHI*, 2021. 1, 2, 3, 6, 7, 9
- [20] Kamal Gupta, Justin Lazarow, Alessandro Achille, Larry S Davis, Vijay Mahadevan, and Abhinav Shrivastava. Layout-transformer: Layout generation and completion with self-attention. *ICCV*, 2021. 1, 2, 3, 6, 7, 9
- [21] Simon Haykin and N Network. A comprehensive foundation. *Neural networks*, 2004. 2
- [22] Kaiming He, Xinlei Chen, Saining Xie, Yanghao Li, Piotr Dollár, and Ross Girshick. Masked autoencoders are scalable vision learners. *CVPR*, 2022. 6, 13
- [23] Kaiming He, Georgia Gkioxari, Piotr Dollár, and Ross Girshick. Mask r-cnn. *ICCV*, 2017. 3
- [24] Martin Heusel, Hubert Ramsauer, Thomas Unterthiner, Bernhard Nessler, and Sepp Hochreiter. Gans trained by a two time-scale update rule converge to a local nash equilibrium. *NeurIPS*, 2017. 7
- [25] Jonathan Ho, Ajay Jain, and Pieter Abbeel. Denoising diffusion probabilistic models. *NeurIPS*, 2020. 2
- [26] Sepp Hochreiter and Jürgen Schmidhuber. Long short-term memory. *Neural computation*, 1997. 2
- [27] Zaeem Hussain, Mingda Zhang, Xiaozhong Zhang, Keren Ye, Christopher Thomas, Zuha Agha, Nathan Ong, and Adriana Kovashka. Automatic understanding of image and video advertisements. *CVPR*, 2017. 6, 13
- [28] Zhaoyun Jiang, Huayu Deng, Zhongkai Wu, Jiaqi Guo, Shizhao Sun, Vuksan Mijovic, Zijiang Yang, Jian-Guang Lou, and Dongmei Zhang. Unilayout: Taming unified sequence-to-sequence transformers for graphic layout generation. *arXiv*, 2022. 2, 3, 7
- [29] Zhaoyun Jiang, Shizhao Sun, Jihua Zhu, Jian-Guang Lou, and Dongmei Zhang. Coarse-to-fine generative modeling for graphic layouts. *AAAI*, 2022. 2, 3
- [30] Akash Abdu Jyothi, Thibaut Durand, Jiawei He, Leonid Sigal, and Greg Mori. Layoutvae: Stochastic scene layout generation from a label set. *ICCV*, 2019. 2, 3
- [31] Tero Karras, Timo Aila, Samuli Laine, and Jaakko Lehtinen. Progressive growing of gans for improved quality, stability, and variation. *ICLR*, 2018. 2, 3
- [32] Tero Karras, Samuli Laine, and Timo Aila. A style-based generator architecture for generative adversarial networks. *CVPR*, 2019. 2, 3
- [33] Tero Karras, Samuli Laine, Miika Aittala, Janne Hellsten, Jaakko Lehtinen, and Timo Aila. Analyzing and improving the image quality of stylegan. *CVPR*, 2020. 2, 3, 13
- [34] Kotaro Kikuchi, Edgar Simo-Serra, Mayu Otani, and Kota Yamaguchi. Constrained graphic layout generation via latent optimization. *ACM MM*, 2021. 1, 2, 3, 4, 5, 6, 7, 9
- [35] Diederik P Kingma and Jimmy Ba. Adam: A method for stochastic optimization. *ICLR*, 2015. 13
- [36] Diederik P Kingma and Max Welling. Auto-encoding variational bayes. *ICLR*, 2013. 1, 2, 5
- [37] Thomas N Kipf and Max Welling. Semi-supervised classification with graph convolutional networks. *ICLR*, 2017. 2
- [38] Xiang Kong, Lu Jiang, Huiwen Chang, Han Zhang, Yuan Hao, Haifeng Gong, and Irfan Essa. Blt: Bidirectional layout transformer for controllable layout generation. *ECCV*, 2022. 1, 2, 3, 6, 7
- [39] Alex Krizhevsky, Ilya Sutskever, and Geoffrey E Hinton. Imagenet classification with deep convolutional neural networks. *NeurIPS*, 2012. 2
- [40] R Landa. Graphic design solutions/robin landa. *Wadsworth, Boston*, 2010. 1
- [41] Anders Boesen Lindbo Larsen, Søren Kaae Sønderby, Hugo Larochelle, and Ole Winther. Autoencoding beyond pixels using a learned similarity metric. *ICML*, 2016. 1, 2, 5
- [42] Donghoon Lee, Sifei Liu, Jinwei Gu, Ming-Yu Liu, Ming-Hsuan Yang, and Jan Kautz. Context-aware synthesis and placement of object instances. *NeurIPS*, 2018. 2
- [43] Hsin-Ying Lee, Lu Jiang, Irfan Essa, Phuong B Le, Haifeng Gong, Ming-Hsuan Yang, and Weilong Yang. Neural design network: Graphic layout generation with constraints. *ECCV*, 2020. 2, 3, 6
- [44] Kwonjoon Lee, Huiwen Chang, Lu Jiang, Han Zhang, Zhuowen Tu, and Ce Liu. Vitgan: Training gans with vision transformers. *ICLR*, 2022. 2, 3
- [45] Elad Levi, Eli Brosh, Mykola Mykhailych, and Meir Perez. Dlt: Conditioned layout generation with joint discrete-continuous diffusion layout transformer. *arXiv*, 2023. 2, 3
- [46] Gang Li, Gilles Baechler, Manuel Tragut, and Yang Li. Learning to denoise raw mobile ui layouts for improving datasets at scale. *CHI*, 2022. 6
- [47] Junnan Li, Dongxu Li, Caiming Xiong, and Steven Hoi. Blip: Bootstrapping language-image pre-training for unified

- vision-language understanding and generation. *ICML*, 2022. 5, 13
- [48] Jianan Li, Jimei Yang, Aaron Hertzmann, Jianming Zhang, and Tingfa Xu. Layoutgan: Generating graphic layouts with wireframe discriminators. *ICLR*, 2019. 1, 2, 3
- [49] Jianan Li, Jimei Yang, Jianming Zhang, Chang Liu, Christina Wang, and Tingfa Xu. Attribute-conditioned layout gan for automatic graphic design. *TVCG*, 2020. 2, 3, 6, 7
- [50] Tsung-Yi Lin, Priya Goyal, Ross Girshick, Kaiming He, and Piotr Dollár. Focal loss for dense object detection. *ICCV*, 2017. 3
- [51] Bingchen Liu, Yizhe Zhu, Kunpeng Song, and Ahmed Elgammal. Towards faster and stabilized gan training for high-fidelity few-shot image synthesis. *ICLR*, 2020. 4
- [52] Shilong Liu, Feng Li, Hao Zhang, Xiao Yang, Xianbiao Qi, Hang Su, Jun Zhu, and Lei Zhang. Dab-detr: Dynamic anchor boxes are better queries for detr. *ICLR*, 2022. 3
- [53] Simon Lok and Steven Feiner. A survey of automated layout techniques for information presentations. *Proceedings of SmartGraphics*, 2001. 1
- [54] Depu Meng, Xiaokang Chen, Zejia Fan, Gang Zeng, Houqiang Li, Yuhui Yuan, Lei Sun, and Jingdong Wang. Conditional detr for fast training convergence. *ICCV*, 2021. 3
- [55] Nelson Nauata, Kai-Hung Chang, Chin-Yi Cheng, Greg Mori, and Yasutaka Furukawa. House-gan: Relational generative adversarial networks for graph-constrained house layout generation. *ECCV*, 2020. 2, 3
- [56] Nelson Nauata, Sepidehsadat Hosseini, Kai-Hung Chang, Hang Chu, Chin-Yi Cheng, and Yasutaka Furukawa. House-gan++: Generative adversarial layout refinement network towards intelligent computational agent for professional architects. *CVPR*, 2021. 2, 3
- [57] David D Nguyen, Surya Nepal, and Salil S Kanhere. Diverse multimedia layout generation with multi choice learning. *Multimedia*, 2021. 2, 3
- [58] Alex Nichol, Prafulla Dhariwal, Aditya Ramesh, Pranav Shyam, Pamela Mishkin, Bob McGrew, Ilya Sutskever, and Mark Chen. Glide: Towards photorealistic image generation and editing with text-guided diffusion models. *ICML*, 2022. 2
- [59] Niki Parmar, Ashish Vaswani, Jakob Uszkoreit, Lukasz Kaiser, Noam Shazeer, Alexander Ku, and Dustin Tran. Image transformer. *ICML*, 2018. 13
- [60] Akshay Gadi Patil, Omri Ben-Eliezer, Or Perel, and Hadar Averbuch-Elor. Read: Recursive autoencoders for document layout generation. *CVPR Workshops*, 2020. 1, 2, 3, 6, 7, 9
- [61] Joseph Redmon, Santosh Divvala, Ross Girshick, and Ali Farhadi. You only look once: Unified, real-time object detection. *CVPR*, 2016. 3
- [62] Joseph Redmon and Ali Farhadi. Yolo9000: better, faster, stronger. *CVPR*, 2017. 3
- [63] Shaoqing Ren, Kaiming He, Ross Girshick, and Jian Sun. Faster r-cnn: Towards real-time object detection with region proposal networks. *NeurIPS*, 2015. 3
- [64] Hamid Rezaatofghi, Nathan Tsoi, JunYoung Gwak, Amir Sadeghian, Ian Reid, and Silvio Savarese. Generalized intersection over union: A metric and a loss for bounding box regression. *CVPR*, 2019. 3, 5
- [65] Danilo Jimenez Rezende, Shakir Mohamed, and Daan Wierstra. Stochastic backpropagation and approximate inference in deep generative models. *ICML*, 2014. 2, 5
- [66] Robin Rombach, Andreas Blattmann, Dominik Lorenz, Patrick Esser, and Björn Ommer. High-resolution image synthesis with latent diffusion models. *CVPR*, 2022. 1, 2
- [67] Tim Salimans, Andrej Karpathy, Xi Chen, and Diederik P Kingma. Pixelcnn++: Improving the pixelcnn with discretized logistic mixture likelihood and other modifications. *ICLR*, 2017. 2
- [68] Axel Sauer, Katja Schwarz, and Andreas Geiger. Stylegan-xl: Scaling stylegan to large diverse datasets. *SIGGRAPH*, 2022. 2, 3
- [69] Karen Simonyan and Andrew Zisserman. Very deep convolutional networks for large-scale image recognition. *ICLR*, 2015. 2
- [70] Richard Socher, Cliff C Lin, Chris Manning, and Andrew Y Ng. Parsing natural scenes and natural language with recursive neural networks. *ICML*, 2011. 2
- [71] Richard Socher, Alex Perelygin, Jean Wu, Jason Chuang, Christopher D Manning, Andrew Y Ng, and Christopher Potts. Recursive deep models for semantic compositionality over a sentiment treebank. *EMNLP*, 2013. 2
- [72] Jiaming Song, Chenlin Meng, and Stefano Ermon. Denoising diffusion implicit models. *ICLR*, 2021. 2
- [73] Mary Stribley. Rules of composition all designers live by. *Retrieved May*, 2016. 1
- [74] Roman Suvorov, Elizaveta Logacheva, Anton Mashikhin, Anastasia Remizova, Arsenii Ashukha, Aleksei Silvestrov, Naejin Kong, Harshith Goka, Kiwoong Park, and Victor Lempitsky. Resolution-robust large mask inpainting with fourier convolutions. *WACV*, 2022. 6, 14, 17
- [75] Fuwen Tan, Crispin Bernier, Benjamin Cohen, Vicente Ordonez, and Connelly Barnes. Where and who? automatic semantic-aware person composition. *WACV*, 2018. 2
- [76] Aaron Van den Oord, Nal Kalchbrenner, Lasse Espeholt, Oriol Vinyals, Alex Graves, et al. Conditional image generation with pixelcnn decoders. *NeurIPS*, 2016. 2
- [77] Ashish Vaswani, Noam Shazeer, Niki Parmar, Jakob Uszkoreit, Llion Jones, Aidan N Gomez, Łukasz Kaiser, and Illia Polosukhin. Attention is all you need. *NeurIPS*, 2017. 2, 6, 13
- [78] Xiaolong Wang, Ross Girshick, Abhinav Gupta, and Kaiming He. Non-local neural networks. *CVPR*, 2018. 6, 13
- [79] Yizhi Wang, Guo Pu, Wenhan Luo, Yexin Wang, Pengfei Xiong, Hongwen Kang, and Zhouhui Lian. Aesthetic text logo synthesis via content-aware layout inferring. *CVPR*, 2022. 2, 3, 6
- [80] Yuxi Xie, Danqing Huang, Jinpeng Wang, and Chin-Yew Lin. Canvasemb: learning layout representation with large-scale pre-training for graphic design. *Multimedia*, 2021. 2, 3

- [81] Kota Yamaguchi. Canvasvae: learning to generate vector graphic documents. *ICCV*, 2021. [2](#), [3](#), [6](#)
- [82] Fenggen Yu, Kun Liu, Yan Zhang, Chenyang Zhu, and Kai Xu. Partnet: A recursive part decomposition network for fine-grained and hierarchical shape segmentation. *CVPR*, 2019. [6](#)
- [83] Jiahui Yu, Xin Li, Jing Yu Koh, Han Zhang, Ruoming Pang, James Qin, Alexander Ku, Yuanzhong Xu, Jason Baldridge, and Yonghui Wu. Vector-quantized image modeling with improved vqgan. *ICLR*, 2022. [2](#), [3](#)
- [84] Ning Yu, Ke Li, Peng Zhou, Jitendra Malik, Larry Davis, and Mario Fritz. Inclusive gan: Improving data and minority coverage in generative models. *ECCV*, 2020. [2](#), [3](#)
- [85] Ning Yu, Guilin Liu, Aysegul Dundar, Andrew Tao, Bryan Catanzaro, Larry S Davis, and Mario Fritz. Dual contrastive loss and attention for gans. *ICCV*, 2021. [2](#), [3](#)
- [86] Fuyang Zhang, Nelson Nauata, and Yasutaka Furukawa. Conv-mpn: Convolutional message passing neural network for structured outdoor architecture reconstruction. *CVPR*, 2020. [3](#)
- [87] Hengshuang Zhao, Xiaohui Shen, Zhe Lin, Kalyan Sunkavalli, Brian Price, and Jiaya Jia. Compositing-aware image search. *ECCV*, 2018. [2](#)
- [88] Xinru Zheng, Xiaotian Qiao, Ying Cao, and Rynson WH Lau. Content-aware generative modeling of graphic design layouts. *TOG*, 2019. [1](#), [2](#), [3](#), [5](#), [6](#)
- [89] Xu Zhong, Jianbin Tang, and Antonio Jimeno Yepes. Publaynet: largest dataset ever for document layout analysis. *ICDAR*, 2019. [6](#)
- [90] Min Zhou, Chenchen Xu, Ye Ma, Tiezheng Ge, Yuning Jiang, and Weiwei Xu. Composition-aware graphic layout gan for visual-textual presentation designs. *IJCAI*, 2022. [1](#), [2](#), [3](#), [6](#), [7](#), [9](#), [16](#)

7. Supplementary material

A. Implementation Details

Architecture design is where we integrate object detection with layout generation. Detection transformer (DETR) architecture [9] is employed and modified for LayoutDETR generator G and conditional discriminator D^c . It targets to boost the understanding of background from the perspective of visual detection, and enhance the controllability of background on the layout.

As depicted in Figure 2 bottom left, G and D^c contain a visual transformer encoder for background understanding and a transformer decoder for layout generation or discriminator feature representation. The encoder part is the same as in DETR [9], and is identical in G and D^c . It consists of a CNN backbone that extracts a compact feature representation from a background image, as well as a multi-head ViT encoder [22, 78] that incorporates positional encoding inputs [6, 59]. It outputs tokenized visual features for cross-attention in the following layout transformer decoder.

The layout decoder is also inherited from the DETR transformer decoder with self-attention and encoder-decoder-cross-attention mechanisms [77]. In G , it transforms each of the N input embeddings (corresponding to N foreground elements) into layout bounding box parameters, whereas in D^c , it transforms each of the N bounding box embeddings into discriminator features. Our architecture differs from DETR where we have foreground elements as inputs to drive the transformation, while DETR does not. Therefore, we replace their freely-learnable object queries with our foreground embeddings as the input tokens to the decoder, which are detailed below.

In G , foreground elements are composed of texts $\mathcal{T} = \{\mathbf{t}^i\}_{i=1}^M = \{(s^i, c^i, l^i)\}_{i=1}^M$ and image patches $\mathcal{P} = \{\mathbf{p}^i\}_{i=1}^K$. Thence, each foreground embedding is a concatenation of noise embedding and either text embedding or image embedding. To calculate the text embedding, we separately encode text string s , text class c , and text length l , and concatenate the features together. The text string is encoded by the pretrained and fixed BERT text encoder [16]. The text class and quantized text length are encoded by learning a dictionary. To calculate the image embedding, we use the same ViT as used for background encoding. The weights are shared and initialized by the Up-DETR-pretrained model [15]. Note that the font color is not considered in the modeling because it is trivial information. According to our empirical observation, font colors are dominated by two and only two modes: black and white. As indicated in Figure 4 caption: Text font colors and button pad colors are adaptively determined to be either black or white whichever contrasts more with the background.

For the other networks F^c , D^u , F^u , E , and R that do not take background images as an input condition, we simply use the above transformer decoder architecture as their

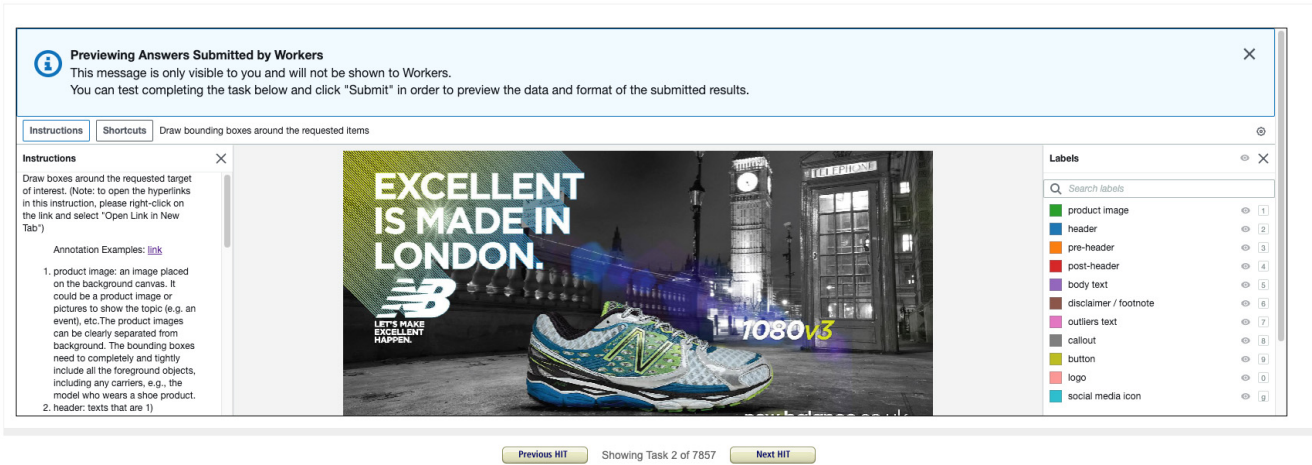
implementations. Following transformers, for each foreground image reconstruction in F^c and R , we employ the StyleGAN2 image generator architecture [33]. For each text string reconstruction, we employ the pretrained BERT language model decoder [16, 47]. For each text class and text length decoding, we use 3-layer MLPs.

We implement LayoutDETR in PyTorch and use Adam optimizer [35] to train the models on 8 NVIDIA A100 GPUs, each with 40GB memory. Because bounding box parameters are normalized by image resolutions, during training and inference we downsize arbitrary images to 256×256 without losing generality. For final rendering and visualization, we resize them back to their original resolutions. Small and unified image size allows us to train models with a large enough batch size, e.g., 64 in our experiments. During training, we set the learning rate constantly as 10^{-5} and train for 110k iterations in 4 days. Inference is much more efficient: we load only G into a single NVIDIA A100 GPU and it consumes only 2.82GB of memory. It takes only 0.38 sec to generate a layout given foreground and background conditions.

B. Details of Our Ad Banner Dataset Collection

The sources of raw ad banner images consist of two parts. First, we manually went through all the images in Pitt Image Ads Dataset [27]. We filtered out those with single modality, low quality, or old-fashioned designs. We then selected 3,536 valid ad banner images. Second, we searched on Google Image Search Engine with the keywords "XXX ad banner" where "XXX" goes through a list of 2,765 retailer brand names including the Fortune 500 brands. For each keyword search, we crawled the top 20 results and manually filtered out non-ads, single-modality, low-quality, or offensive-content images. We then selected 4,321 valid ad banner images. Combining the two sources, we in total obtained 7,857 valid ad banner images with arbitrary sizes.

Next, we crowdsourced on Amazon Mechanical Turk (AMT) [2] to obtain human annotations for the bounding box and class of each text phrase in each image. The class space spans over 11 categories as shown in the AMT interface in Figure 5 top. Without losing representativeness, we focus on the top-4 most common categories in this work: $\{header, body\ text, disclaimer / footnote, button\}$. We also linked a detailed instructional document with examples for workers to fully understand the annotation task. See the instruction in Figure 5 bottom. We assigned each annotation job to three workers. For the final annotation results, we averaged over three workers' submissions and incorporated our judgments for the tie cases. In total there were 67 workers involved in the task. On average each worker submitted 314 jobs in around 3 minutes per job. All of the workers have an approval rate history above 90% on AMT. We did not set any restrictions for workers' gender, race, sexuality, demographics, locations, remuneration rates, etc. Our



(a) AMT interface



Product image: need to completely and tightly include all the foreground objects, cannot go outside the banner canvas

(b) Instructional example

Figure 5. **Top:** AMT interface with instructions on the left for users to annotate the bounding box and class of each existing copywriting text on each image. **Bottom:** one instructional example of the definitions of text bounding boxes and text classes.

annotation process has been reviewed and approved by our ethical board.

After annotation, it is necessary to reverse the design by separating foreground elements from background images to configure the training/testing data. We apply a modern optical character recognition (OCR) technique [1] to extract the text inside each bounding box, and adopt a modern image inpainting technique [74] to erase the texts. The separation of texts from background images is exemplified in Figure 6. After filtering out a few samples with undesirable OCR or inpainting results, we finally obtain 7,196 valid samples for the following experiments.

It is worth noting that inpainting clues may leak the lay-

out bounding box ground truth information and shortcut training. Therefore, during training, we intentionally inpaint background images at additional random subregions that are irrelevant to their layouts.

C. Graphical System Step-by-Step Designs

Since we validate that our solution sets up a new state of the art for multimodal layout design, it is worth integrating it into a graphical system for user-friendly service in practice. Figure 7 demonstrates our step-by-step UI designs. In specific:

(1) Figure 7(a) shows the initial page that allows users to customize their background images and option-

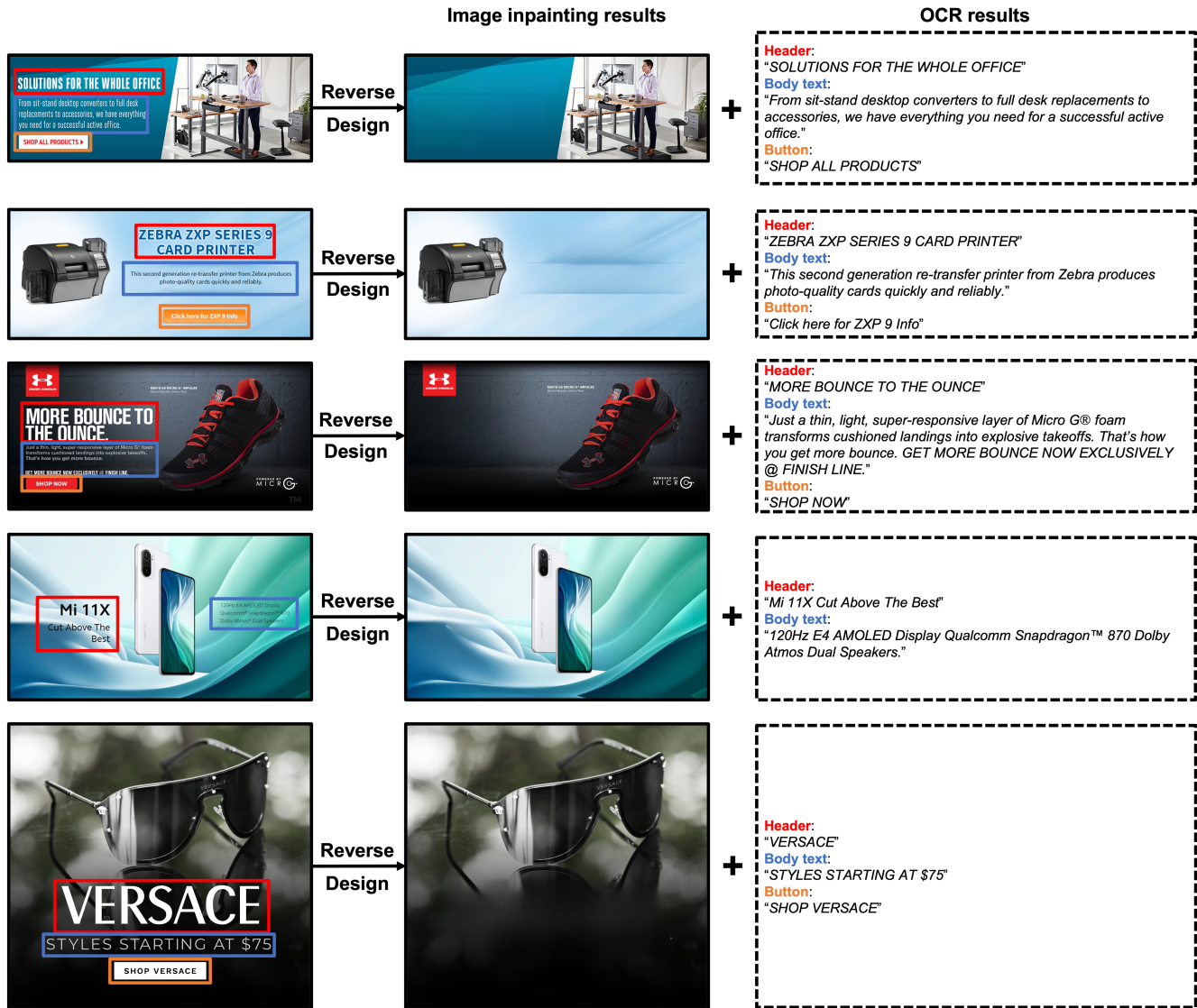


Figure 6. Reverse engineering examples of separating foreground elements from background images using OCR and image inpainting techniques.

ally foreground elements: *header text*, *body text*, *foot-note/disclaimer text*, *button text*, as well as *button border radius* (zero radius means a rectangular button). Text colors, button pad colors, and text fonts can also be customized.

(2) Once users upload their background and foreground elements, they are previewed on the right part of the same page, as shown in Figure 7(b). The locations and sizes of foreground elements in the preview are meaningless: they just conceptually show what contents are going to be rendered on top of the background.

(3) Once users click "Next", it moves on to the next page with our design results, as shown in Figure 7(c). Given one layout designed in the backend, we post-process it by randomly jittering the generated box parameters by 20% while

keeping the original non-overlapping and alignment regularity.

(4) Afterwards, the system renders foreground elements given the layout bounding boxes. Text font sizes and line breakers are adaptively determined so as to tightly squeeze into the boxes. Considering *header texts* usually have short strings yet are assigned with large boxes, their font sizes are naturally large enough. Text font styles can also randomly vary. We showcase six of our rendered results on this page, and allow users to select one or more satisfactory designs.

(5) Once users make their selection(s) and click "Save Selection", it moves onto the last page as shown in Figure 7(d). On this page, users are allowed to manually customize the size and location of each rendered foreground element.

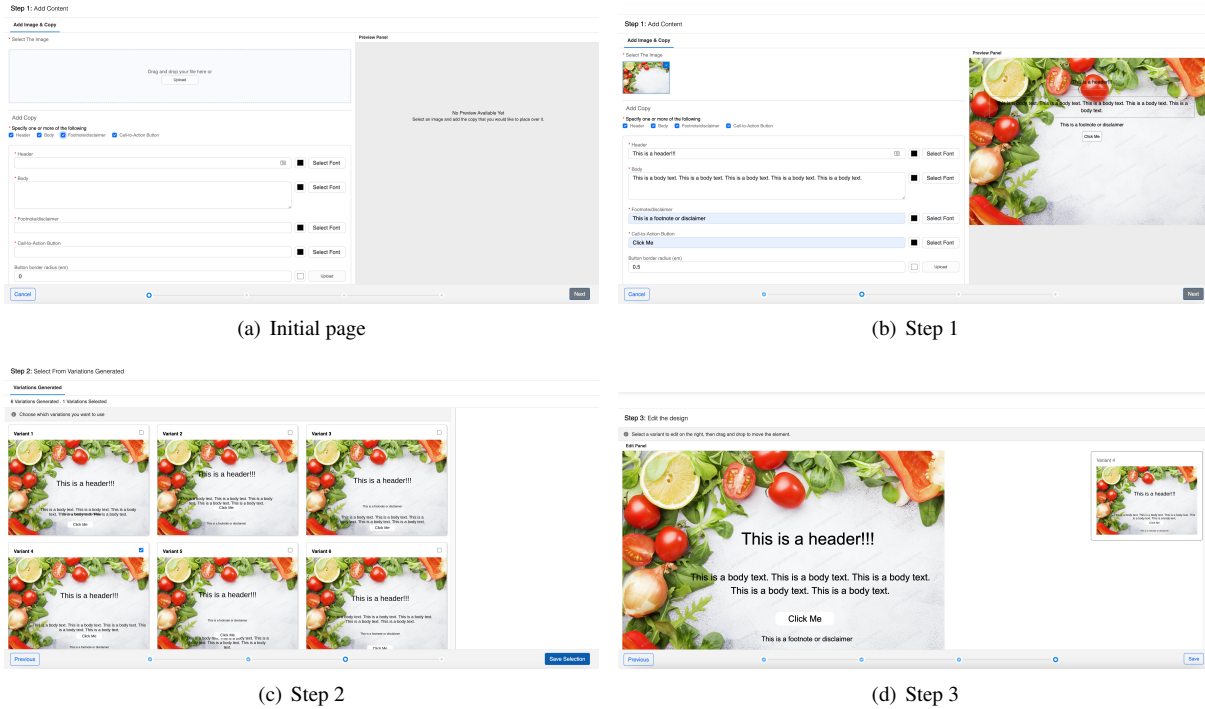


Figure 7. Step-by-step usage of our graphical system for customizable multimodal graphic layout design.

Once they finish, they click "Save" to exit our system.

D. More qualitative results

We show in Fig. 8 more uncurated qualitative results of layout designs and text rendering on background images in the wild and on CGL Chinese ad banner inpainted background [90]. Conditioned on multiple text inputs in varying categories, our designs appear aesthetically appealing and harmonic between foreground and background.

We show in Fig. 9 the impact of varying texts on layouts given the same background image. We observe: (1) the scales of bounding boxes are adaptively proportional to the varying lengths of texts such that the font sizes remain approximately unchanged, and (2) the global and relative locations of bounding boxes are stable regardless of the changes of texts, which are reliably harmonic with the background structure.

E. Limitation on Challenging Samples

We show in Fig. 10 a few imperfect layout designs for challenging samples. When the background images are over-clutter and texts are wordy, none of our rendering variants looks very ideal. Our model struggles between (1) placing layouts in the middle regardless of background and (2) placing layouts over less busy areas at edges that breaks the spatial balance. A possible workaround could be introducing gradient blending masks into the rendering post-processing.

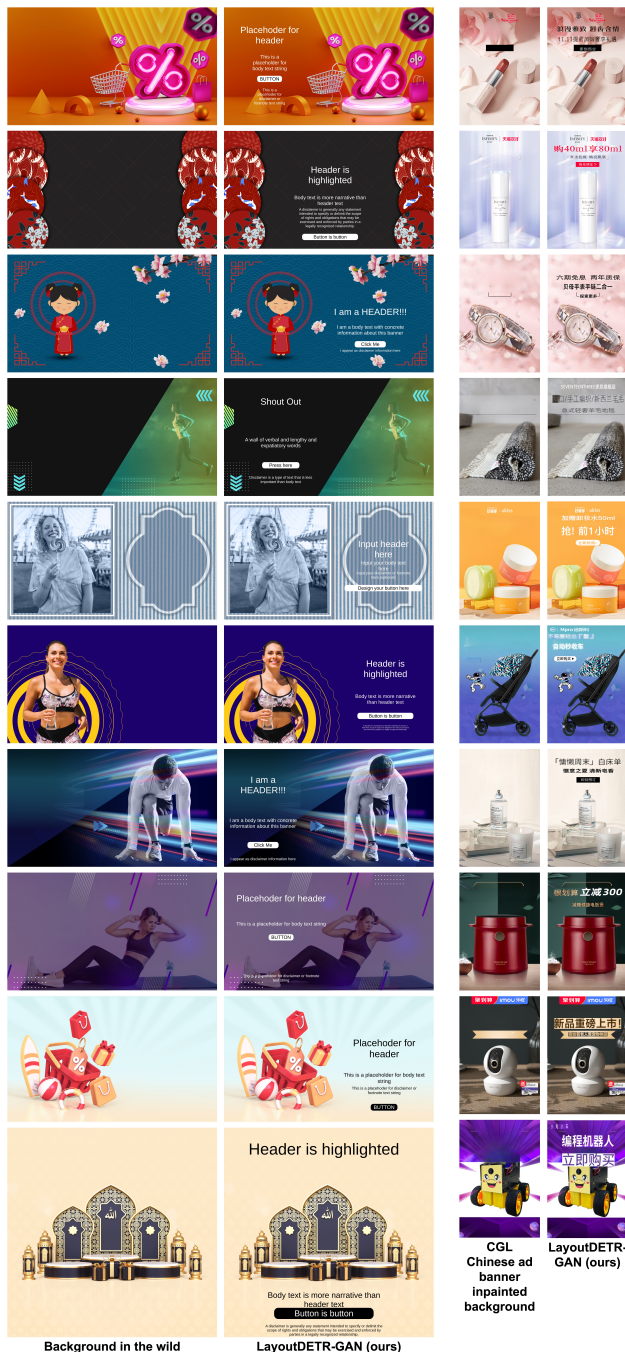


Figure 8. **Left:** uncurated layout designs and text rendering on background images in the wild (extracted from PSD data downloaded from [3] with searching keywords “ad banner”). Rendering rules: (1) Text font sizes and line breakers are adaptively determined to tightly fit into their inferred boxes. (2) Text font colors and button pad colors are adaptively determined to be either black or white whichever contrasts more with the background. (3) Button text colors are then determined to contrast with the button pads. (4) Text font is set to *Arial*. **Right:** uncurated layout designs and text rendering on CGL Chinese ad banner background images inpainted by [74]. Image patches that contain foreground text elements are resized and overlaid on the background following the generated layouts.



Figure 9. **Top:** ad banner design given the same background image (downloaded from [4]) and varying text combinations. **Bottom:** ad banner design given the same background image and varying only the *header* text component.



Figure 10. Imperfect layout designs for over-clutter background images and wordy texts. Image sources are from [4].